Geophys. J. Int. (2000) **140,** 295–310

Natural gas hydrates on the continental slope off Pakistan: constraints from seismic techniques

Ingo Grevemeyer,* Andreas Rosenberger and Heinrich Villinger

Fachbereich Geowissenschaften, Universität Bremen, Postfach 33 04 40, 28334 *Bremen, Germany. E-mail: ingo@geophys2.uni-bremen.de*

Accepted 1999 September 6. Received 1999 July 27; in original form 1999 January 25

SUMMARY

In October 1997, new vertical-incidence, wide-angle reflection and refraction data were obtained on the convergent continental margin off Pakistan. The most prominent feature across the entire margin into the Gulf of Oman is a bottom simulating reflector (BSR). This reflection generally coincides with the depth predicted for the base of the gas hydrate stability field. On the accretionary prism the BSR is a clear reflection with inverse polarity, and strata beneath the BSR show enhanced reflectivities, suggesting that gas is trapped between stratigraphic layers. Joint inversion of wide-angle and refraction data yielded a $\sim$200 m thick low-velocitiy zone at BSR depth. Using the Born expansion, band-limited impedance logs were calculated from deconvolved and scaled single-channel data, suggesting that velocity at the BSR drops by $\sim$200 m s^{-1}. Some 40 km towards the coast, CDP4400 of Minshull & White (1989) yielded a velocity inversion of about 600 m s^{-1}, indicating that BSR characteristics vary significantly across the continental margin off Pakistan.

Beneath the Gulf the BSR was sampled at a similar subbottom depth, where seismic bright spots occur. However, its reflection amplitude is unusually low and seismic stratigraphy beneath the BSR did not show enhanced reflectivities. Joint traveltime inversion of wide-angle and refraction data revealed continuously increasing velocities, suggesting that an adequate supply of methane for forming free gas and gas hydrate is mainly confined to sediments incorporated into the accretionary prism. We believe that these variations are related to an evolutionary process due to tectonic uplift and ongoing sedimentation as sediments are incorporated into the accretionary prism. Sedimentation and uplift produce an upward migration of isotherms and therefore lead to a dissociation of gas hydrates, which releases methane gas and thus causes an enhancement of the BSR. Our survey imaged BSR properties of the abyssal plain and within the first slope basin at water depths of 3300 m and 2490 m, respectively. CDP4400 was located farther landwards at a depth of 1730 m within a buried and uplifted and hence more evolved slope basin. We therefore suggest that, in the accretionary wedge, tectonic uplift and ongoing sedimentation cause hydrate recycling by upward migration of the stability field. In addition, tectonic dewatering may accumulate hydrate at the base of the stability field by advection of methane from depth.

Key words: continental margins, gas hydrate, sedimentation, seismic structure, seismic velocities, tectonics.

INTRODUCTION

Natural gas hydrates (clathrates) are a crystalline form of water and gas molecules (mostly methane) that are stable above 0 °C at sufficiently high pressure. Although most of the ocean floor is within the appropriate pressure–temperature regime for gas hydrates to be stable, adequate gas supplies for hydrate formation normally occur only in continental slope regions. In models of gas hydrate formation (e.g. Kvenvolden 1993; Minshull *et al.* 1994), the methane is considered to be mainly microbial, although the significance of thermogenic methane

* Also visiting scientist at GEOMAR, Forschungszentrum für Marine Geowissenschaften, Kiel, Germany.

has been suggested. The concentration of thermogenic methane, however, is usually very low. Regarding the significance of natural gas hydrates, a wealth of ideas has been presented (for a review see Kvenvolden 1993): (1) methane trapped in hydrates may constitute a source of natural gas as a clean-burning fuel; (2) because methane is a greenhouse gas, hydrates may have a major impact on the global climate system; and (3) hydrates may dissociate and cause slope failure on continental margins.

The gas hydrate stability zone (HSZ) is limited to the upper hundreds of metres of the ocean floor beneath which temperatues are too high for hydrates to exist. In seismic data, the base of the hydrate stability zone (BHSZ) is often marked by a bottom simulating reflector (BSR) if gas hydrates or free gas are present. This reflector follows the shape of the seabed and often cuts across the stratigraphy of sediments. Strata above BSRs sometimes show reduced reflectivities (Paull & Dillon 1981; Lee *et al.* 1994), a phenomenon called 'amplitude blanking', which has been associated with the presence of hydrates (Dillon *et al.* 1993). However, recent evidence from Ocean Driling Program (ODP) leg 164 on the Blake Ridge (Holbrook *et al.* 1996) has demonstrated that the low reflectivity in the HSZ is caused by very uniform sediments, and the thick zone of higher reflectivity beneath the BSR marks an unexpectedly thick zone of gas layers. *P* velocity decreases strongly in the presence of small quantities of free gas; thus, the reflectivity seen at and beneath the BSR indicates layers containing trapped gas in pore fluids along stratigraphic layers (Holbrook *et al.* 1996). Reflectivities above the BSR are consequently normal while reflectivities beneath are enhanced.

Reflections from the BSR itself are characterized by high amplitude and inverse polarity with respect to the seafloor reflection, indicating that they represent a strong decrease in acoustic impedance. These properties may be due either to sediment containing small amounts of hydrates overlying a thin low-velocity free gas zone (Minshull & White 1989; Singh *et al.* 1993; Katzman *et al.* 1994) or to a thin high-velocity hydrate zone above (Hyndman & Spence 1992).

The purpose of this study is to investigate the hydrate and free-gas distribution within slope sediments off Pakistan using high-resolution seismic techniques, including vertical-incidence, wide-angle and refraction seismics. Our data are of high quality and supplement earlier single-channel and multichannel profiles (White & Klitgord 1976; White 1977; Minshull & White 1989). The reflection data presented in this paper demonstrate that the BSR is laterally discontinuous; however, the prominent reflector could be imaged across the entire Makran margin. Beneath the abyssal plain the vertical-incidence reflection data show a BSR at a similar subbottom depth where seismic 'bright spots' occur (White 1977; Minshull & White 1989). Neverthless, a joint inversion of vertical-incidence, wide-angle and refraction data yields profound differences between properties of sediments from the Makran accretionary complex and the abyssal plain, which may indicate that an adequate supply of methane for hydrate formation is mainly confined to the accretionary wedge.

GEOLOGICAL SETTINGS

The Makran subduction zone off Pakistan marks a zone of convergence between oceanic lithosphere of the Arabian plate and continental lithosphere of the Eurasian plate (Fig. 1). Measurements of heat flow and basement depth suggest an age of 70–100 Myr for the subducting oceanic crust (Hutchison *et al.* 1981; Kaul *et al.* 2000), and the apparent absence of magnetic spreading anomalies may therefore represent the Cretaceous Magnetic Quiet Zone. The deformation front of the Makran accretionary prism lies $\sim$150 km offshore (Kukowski *et al.* 2000); the accreted wedge continues some 400–500 km farther north across the Makran of Iran and Pakistan.

A large terrigenous sediment supply has created a 7-km thick incoming sediment pile in the Gulf of Oman (White & Louden 1982). Initially gently dipping sediments beneath the abyssal plain become folded at the deformation front and subsequently uplifted as they are incorporated into the accetionary wedge. Landwards of the deformation front, series of east–west-trending folds and faults have been formed (Fig. 1; Kukowski *et al.* 2000). The slope basins between successive thrust slices show evidence for continued tectonic activity (Fig. 2). Bedding planes in the basins dip more steeply landwards with depth, suggesting back-rotation due to thrust reactivation, and curve into faults, suggesting fault drag (Minshull *et al.* 1992). Northwards towards the coast, the pattern of open ridges and basins continues until the ridge tops become buried by subsequently deposited sediment (White & Louden 1982).

A prominent feature across the entire Makran accetionary prism is a BSR (Fig. 2), which appears at a depth of 500–800 m beneath the seafloor (Minshull & White 1989). Seismic modelling has suggested that free gas is trapped beneath the BSR and beneath abyssal plain 'bright spots', which have a similar subbottom depth and inferred origin (White 1977; Minshull & White 1989). The BSR is often distorted in the region of thrusts. On the landward side of slope basins, it no longer mimics the seafloor, but curves upwards. This observation may suggest a temperature anomaly due to the presence of warm pore fluids (Minshull & White 1989; Minshull *et al.* 1992). However, geothermal measurements do not indicate strong systematic variations across slope basins which would support increased fluid flow through bounding faults (Kaul *et al.* 2000).

DATA DESCRIPTION

The data used in this study are vertical-incidence reflection data and ocean bottom hydrophone (OBH) data, obtained in October 1997 during leg 124 of the German research vessel *Sonne* in the Gulf of Oman (Fig. 1). On two profiles, vertical-incidence and OBH data were collected simultaneously using a 2.5-litre generator/injector (GI) airgun shot every 10 s to provide a shot spacing of 25 m. The lines 9705 and 9707 are located in the abyssal plain and on the accretionary wedge, respectively (Figs 1 and 3). Line 9707 was shot a second time, using an 8-litre Prakla airgun operated at 20 s intervals ($\sim$50 m shot spacing), to sample crust beneath a possible low-velocity layer associated with the BSR. The OBH lines were acquired to assess the amount of gas hydrates stored in slope sediments. To delineate lateral variations in the character of the BSR, three reflection profiles were shot perpendicular to the accretionary complex.

The 16 channels of a 100-m array were stacked to a single trace and sampled at 6 kHz initially. Wide-angle and refraction data were recorded on prototype OBHs, supplied and operated

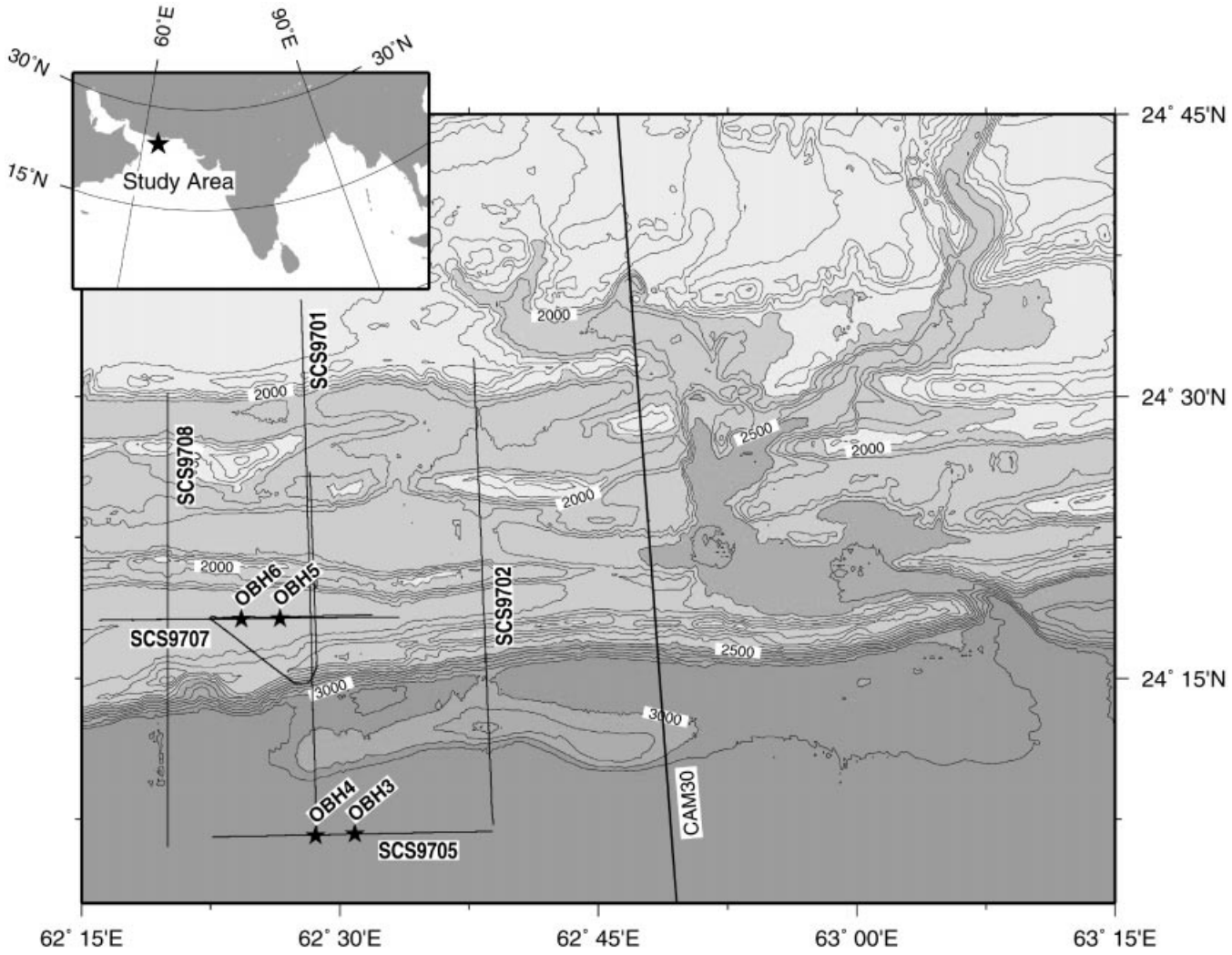

Figure 1. Location map of the seismic survey off Pakistan. Topography is from a HYDROSWEEP swath mapping survey (Kukowski *et al.* 2000). Seismic lines are the solid lines. Ocean bottom hydrophone (OBH) locations are marked by stars. Also shown is the CAM30 line of Minshull & White (1989).

by the Institute of Geophysics, University of Hamburg. OBH data were stored at 24 kHz onto DAT-tapes. Both data sets were anti-alias filtered and resampled at 500 Hz.

A variety of phenomena have been associated with BSRs observed in seismic reflection data, including the inverse polarity of the reflection from the BHSZ, indicating a drop of impedance, and enhanced reflectivity immediately below the BSR reflection. The prime feature, by which a BSR is easily identified, however, is its unconformity with the stratigraphy of the sedimentation; BSR reflections parallel the seafloor reflection with an average 600 ms to 800 ms delay in two-way traveltime (TWT) in the survey area.

All these phenomena can be observed in our single-channel data, although their appearance is highly variable on a local scale (Figs 2 to 4). At some places the BSR is a discrete, reverse and clear reflection, while at other locations it is a low-amplitude reflection only, or it disappears (Fig. 4a). Nevertheless, overall the BSR is continuously present across the entire margin, although the reflector appears to shallow beneath ridges (Figs 2, 4a and b), which are associated with thrust faults (Minshull & White 1989; Minshull *et al.* 1992). Minshull *et al.* (1992) suggested that this behaviour may be attributed to an enhanced thermal gradient due to advective heat flow concentrated in fault zones.

Line 9707 was shot along a slope basin. Like the profiles across the accretionary complex, the data indicate that the BSR is laterally discontinuous. At some locations the reflector is characterized by a clear reverse reflection, while at others it merely marks a transtion from normal-reflectivity sediment to high-reflectivity sediment below (Figs 3, 4d, 4e and 5). In regions where the strata dip through the BHSZ, the BSR has a shingled appearance (Fig. 4e). Here, enhanced reflectivities are a very striking feature and could be observed within a 200–300 ms thick zone (Figs 4e and 5). In addition, depth variations of the BSR (compare Figs 4d and e) indicate lateral variations of the thermal gradient. Compared with profiles crossing the slope basin perpendicularly, line 9707 resolves strata above and below the BSR much better. Strata above and below the BHSZ may produce destructive and constructive interference effects and thus control the seismic appearance of the BSR. Furthermore, variations in the thickness of a free-gas zone beneath a zone where gas hydrate fills some fraction

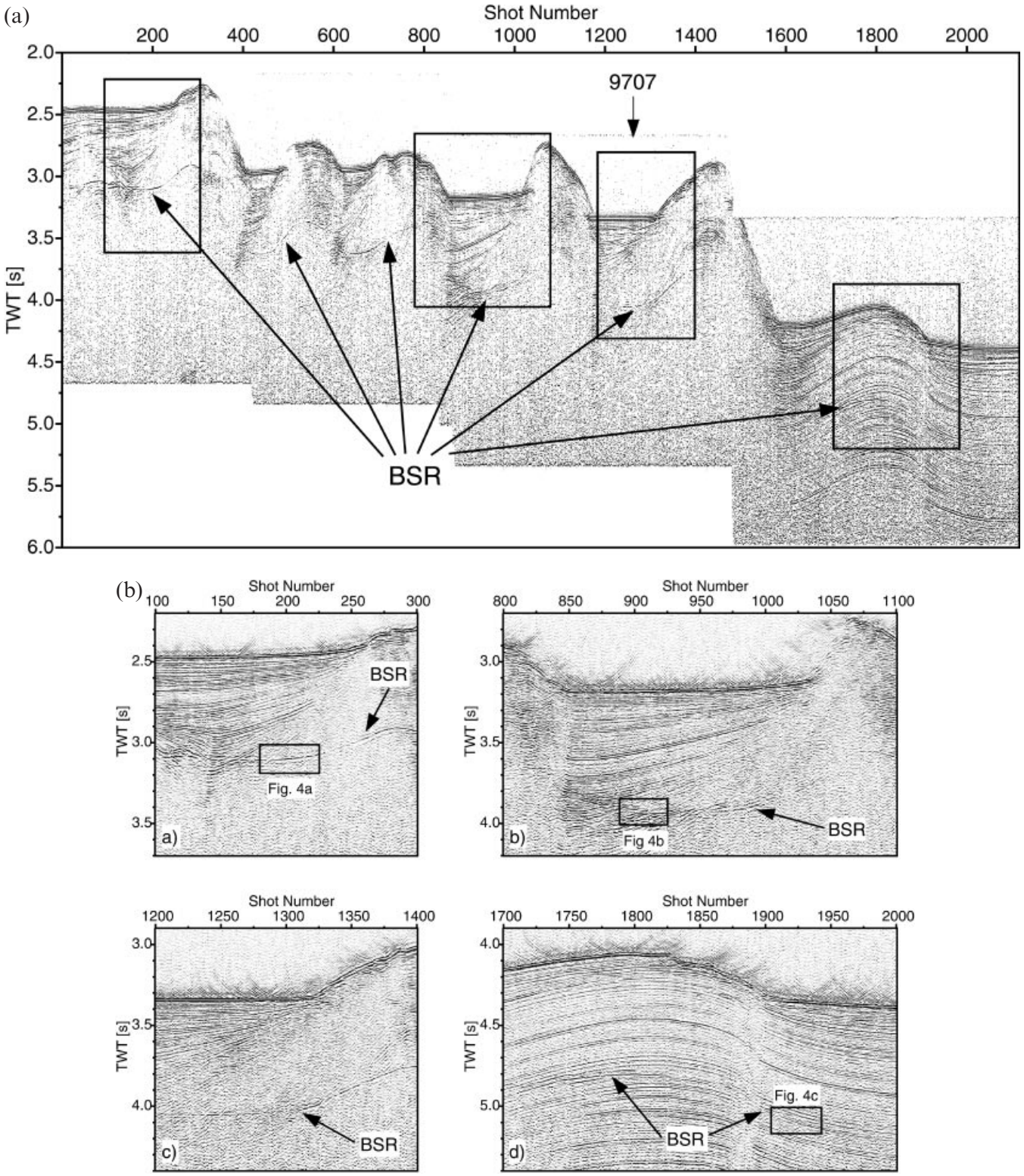

Figure 2. (a) Seismic line 9701 across the active continental margin off Pakistan. Characteristic of the Margin are series of east–west-trending folds and faults (Fig. 1). At 600–800 ms TWT beneath the seafloor the BSR occurs. The prominent reflector roughly mimics the shape of the seabed. Close ups of the four boxes are shown in (b). (b) Time-migrated close ups of line 9701. The BSR can be easily identified by its unconformity with the stratigraphy. With repect to the seafloor, the depth to the BSR increases with increasing water depth from ~600 ms TWT at the most landward site investigated (a) to ~800 ms TWT at the deformation front (d).

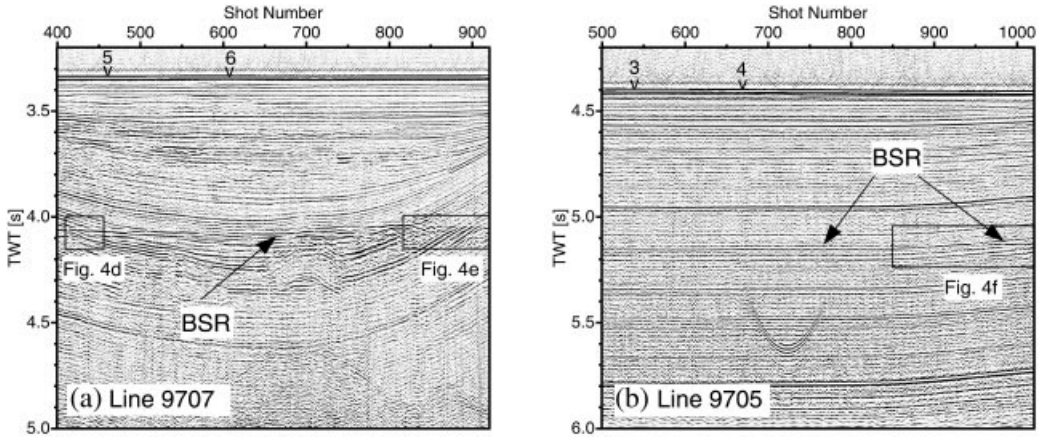

Figure 3. (a) Time-migrated reflection data from line 9707 shot along the first slope basin, and (b) line 9705 located in the Oman abyssal plain. The BSR occurs at 4.06 s TWT and 5.13 s TWT, respectively.

of the porosity may cause lateral variations in BSR appearance (e.g. Miller *et al.* 1991; Lee *et al.* 1994).

Examples of the large-aperture data from line 9707 are shown in Figs 6(a), 7(a) and 7(b). We were able to identify several wide-angle phases between the direct wave and the BSR, which appears as a prominent reflection. A striking feature of the refraction data is that the GI airgun did not transmit energy to offsets larger than 6500 m, while the 8-litre Prakla airgun shows clear arrivals at even larger offsets. Moreover, the data from the 8-litre airgun provided evidence for a low-velocity zone. Therefore, the energy provided by the GI airgun was probably not sufficient to penetrate the low-velocity layer. Nevertheless, the higher frequencies and hence shorter wavetrains of the GI airgun provided a much better resolution of arrivals near the critical distance and of secondary refracted arrivals, which can be used along with the wide-angle data to model the velocity structure within the HSZ.

Seismic reflection data from the frontal fold show a BSR which cuts across the stratigraphy of folded sediments; however, the BSR does not show a strong reflection amplitude (Fig. 4c). The same holds for the BSR imaged beneath the abyssal plain (Fig. 4f), where the reflector occurs at a similar subbottom depth to seismic 'bright spots' (White 1977; Minshull & White 1989). Neither location, however, shows enhanced reflectivity below the BHSZ, and the BSR is only identified because of its strata-cutting character. Nevertheless, we believe that a single layer cutting across parallel running layers does not indicate a minor stratigraphic unconformity, but is a striking feature of a BSR.

The wide-angle and refraction data from line 9705 show several wide-angle phases (Fig. 6b), and the refraction data (Fig. 7c) show that the GI airgun source transmits energy out to offsets of 7800 m. The data, however, do not indicate a BSR and do not provide any evidence for a low-velocity zone associated with high-velocity gas hydrate above, or free gas beneath the BSR. Therefore, major differences between the properties of sediments from the abyssal plain and sediments incorporated into the accretionary wedge are evident.

A striking difference between our single-channel data and data from the multichannel survey of Minshull & White (1989) is the strength of the observed BSR reflection. Minshull & White (1989) observed reflection amplitude ratios of almost 60 per cent for the BSR with respect to the seafloor reflection in stacked multichannel data; Hyndman & Davis (1992) observed ratios of 25–50 per cent in their analysis of multichannel data from the Cascadia accretionary wedge. Generally, amplitudes of the BSR in our data do not exceed 25 per cent of the amplitude of the seafloor reflection. It should be pointed out that our data and the data of Minshull & White (1989) have different spectral properties. Our data acquisition was partially impaired due to strong low-frequency streamer noise. The uncontaminated band is limited to 30–85 Hz. The stacked data of Minshull & White (1989) have a usable spectrum between 10 and 60 Hz.

METHODOLOGY AND RESULTS

Travetime inversion

Sediment velocities above the BSR should be an important indicator for the distribution of hydrates in this zone. The compressional wave velocity of pure gas hydrate is approximately 3300–3800 m s^{-1} (Whalley 1980; Sloan 1990). The formation of gas hydrate in sediments involves the replacement of pore fluid with solid gas hydrate, and therefore high velocities above the BSR can indicate a high concentration of hydrates there. Recent studies have demonstrated that the joint traveltime inversion of vertical-incidence and wide-angle reflections is a useful tool for studying gas-hydrate-bearing sediments (Katzman *et al.* 1994; Korenga *et al.* 1997). The vertical-incidence data provide no constraints on seismic velocities, but their spatially dense sampling supplies clear structural information. The wide-angle data do not produce a clear structural image, but can be used to constrain an average velocity model. An assessment of the vertical velocity gradient from seismic reflection data is impossible. The incorporation of seismic refraction data, however, can overcome this problem.

OBHs were deployed by free fall using the Differential Global Positioning System (DGPS) for drop-point positioning. The instrument locations were further constrained using water path arrival times from the airgun shots while the ship was navigated with DGPS. The timing and positioning uncertainties inherent in OBH data are about 10 ms. The good quality of arrivals made picking of the wide-angle and refraction arrivals relatively straightforward. Most arrivals could be picked to ± 10 ms, or better. Both the seismic reflection data

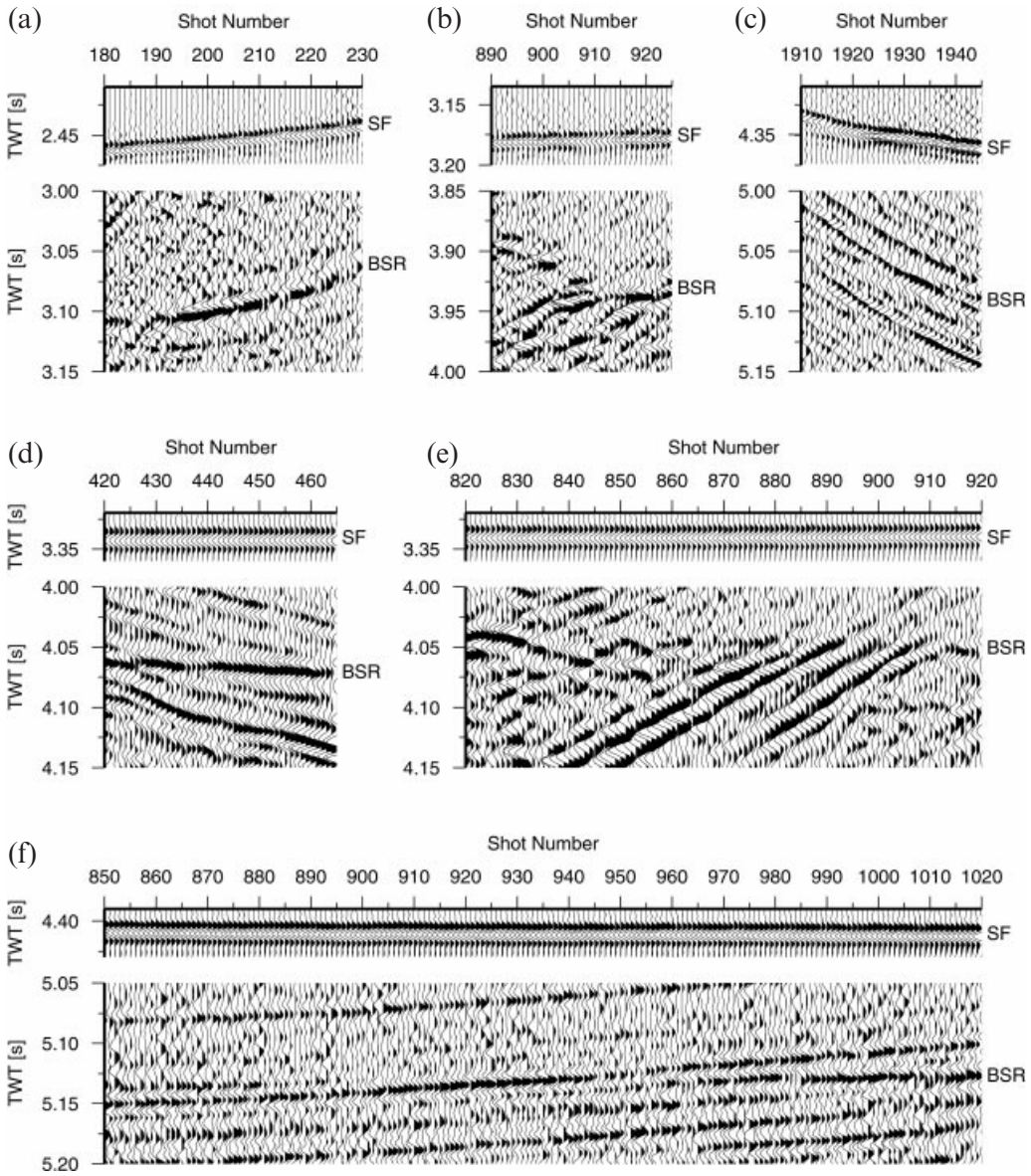

Figure 4. Time-migrated blow ups of seafloor and BSR reflections. Panels (a) to (c) are from line 9701. In regions where the BSR approaches thrusts, the reflector is often distorted. In panels (a) and (b) the thrust is on the right-hand and left-hand sides, respectively. (c) shows the BSR cutting through the strata folded at the deformation front. Panels (d) and (e) are from line 9707, shot along a slope basin; panel (f) from line 9705 shows the BSR in the Gulf of Oman.

and wide-angle reflections transformed into the $X^2 - T^2$ domain indicate almost plane layers of zero dip. Therefore, a τ–p inversion might be an appropriate approach to yield seismic velocities. The τ–p inversion, however, requires that we transform data from the x–t to the τ–p domain. Unfortunately, waveforms from the GI airgun data are often inconsistent between adjacent shots. The incompleteness of the field may result in transform artefacts. In addition, the τ–p inversion breaks down when the seismic velocity drops with increasing depth, as at BSR depth. We therefore choose a 1-D traveltime inversion that uses the picked traveltime data. A velocity model that can satisfy both wide-angle reflection and refraction data was constructed using an iterative, damped least-squares inversion (Zelt & Smith 1992). Furthermore, this approach allows us to include *a priori* information about the drop in velocity at BSR depth.

On profile 9707 along a slope basin of the accretionary wedge, we were able to identify 10 reflectors and five refraction branches. Three branches occur as secondary arrivals; however, they can be readily identified in the GI airgun record sections (Fig. 7a). Velocities within the layer above the BSR are constrained by the wide-angle reflection from the BSR and by a clear first arrival refraction branch. In order to obtain an estimate of the uncertainty of its velocity, we perturb the velocity and observe the resulting rms traveltime residuals for both refracted and reflected arrivals (Fig. 8). From this we conclude that the average velocity in this layer is 2300 m s^{-1}, which is about 100 m s^{-1} faster than for a single gradient background model (Fig. 9) and may indicate the replacement of pore fluid with solid gas hydrate.

In general it is difficult to construct a low-velocity zone from traveltime data alone. Nevertheless, we can infer a physically

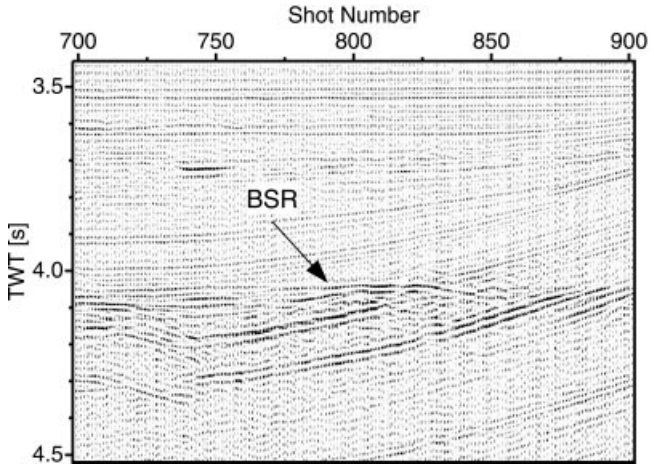

Figure 5. Time-migrated image from line 9707 to show the increase in reflectivity beneath the BSR.Enhanced reflectivities are interpreted in terms of small quantities of free gas trapped along stratigraphic layers beneath the hydrate stability field.

reasonably model when we consider results from previous studies. BSRs are characterized by negative reflection coefficients, indicating a negative acoustic impedance contrast that may be due (1) to sediments containing small amounts of hydrate overlying a low-velocity free-gas zone (Minshull & White 1989; Singh *et al.* 1993; Katzman *et al.* 1994), or (2) to abnormally high-velocity hydrated sediments overlying water-saturated sediments (Hyndman & Spence 1992). Assuming that the 2300-m s^{-1} layer right above the BSR represents a zone of hydrate-bearing sediments, we first drop the velocity beneath the BSR to the value of the 2200-m s^{-1} layer immediately above the hydrate zone. Again we invert the traveltimes. Ignoring the low-velocity zone, the resulting velocity–depth profile could be easily approximated by a single vertical velocity gradient. We therefore suggest that the model is a good approximation of the background velocity structure. Nevertheless, additional data are necessary to assess the velocity beneath the BSR more precisely. We therefore calculated band-limited impedance logs (see the following section), which suggested a drop in the *P* velocity of about 200 m s^{-1}. We used this value to invert again the traveltime data for rays turning beneath the BHSZ. The resultant velocity–depth model is shown in Fig. 9.

Line 9707 in the abyssal plain provided eight good wide-angle reflections. In the refraction data, we found no evidence for strong secondary arrivals. Therefore a single vertical gradient model was found which fits the refraction data as well as the velocity profile obtained from the joint analysis (Fig. 9). In contrast to the case for data from the accretionary prism, we did not find any evidence of hydrated sediments or of free gas associated with a low-velocity zone.

Fig. 9 shows the velocities from the joint traveltime inversion and velocity estimates of the Makran accretionary wedge and Gulf sediments using pre-stack depth migration with error focusing analysis of multichannel seismic data (Frühn *et al.* 1997). Both surveys provide essentially the same models, although the velocity–depth solutions from the seismic reflection data may present a homogeneous layer approximation of our solution obtained by joint traveltime inversion of large-aperture data.

Band-limited impedance logs

To facilitate the discussion of the seismic reflection data we computed band-limited impedance logs at a location coincident with the deployment of the ocean bottom hydrophones on the accretionary prism. The data processing required to derive a band-limited impedance log from a vertical-incidence seismogram is illustrated in Appendix A. Originally, the algorithm was described in Dorau (1991).

A prerequisite for the application of the sparse spike-train deconvolution of Levy & Fullagar (1981) is the estimation of a source wavelet from the data. This estimate needs to be reasonably accurate within the spectral band used to constrain the solution. The usable spectral band in turn is limited by the noise present in the data. Spectral bandwidth (and thus resolution) has to be traded against noise tolerance. The resulting deconvolved trace carries contributions to reflectivity from impedance discontinuities only; gradients and any higher-order, continuous impedance changes are not mapped. Thus, the low-frequency trend in particular of the impedance function is lost and has to be reconstructed using the results from traveltime inversion of the OBH data, and a regional density–depth relationship has to be derived from a porosity–depth function such as that given by Minshull & White (1989) (Fig. 10a). The resulting background impedance log is given in Fig. 10(b), and the two-way traveltime versus depth relationship derived from the velocity model in Fig. 9(a) is depicted in Fig. 10(c).

The computation of band-limited impedance logs from the deconvolved data is based on the Born expansion (e.g. Lavergne & Willm 1977; Clayton & Stolt 1981; Dietrich & Kormendi 1990), which is a valid approximation for a plane wave scattering problem. Consequently, the data have to be scaled to compensate for spherical spreading. Absolute scaling is required as well, and is accomplished assuming a seafloor reflection coefficient of 0.19–0.2, which is in reasonably good agreement with estimates from White (1977).

Fig. 11(a) shows a subset of data from profile 9707 close to the positions of OBH5 and OBH6. At 4.03 s, the BSR is cutting through slightly dipping layers. Two adjacent traces, trace 454 and trace 455, as marked by the arrow in Fig. 11(a), were used to compute the band-limited impedance logs in Fig. 12(b). Resolution is limited by the spectral constraints and by the noise to the frequency band from 40 to 85 Hz, equivalent to 22 ms in the time domain.

Fig. 11(b) illustrates how minor discrepancies in the two traces give rise to noticeable deviations in band-limited impedance; the general features, however, agree very well. To show that the band-limited impedance log in Fig. 11(b) is a model which in fact explains the measured data without major contradictions, we use it to compute a synthetic trace by means of a plane wave reflectivity algorithm which includes transmission losses and all multiples, and convolve the reflectivity function with the estimated wavelet. The result (thick black line) is plotted against the measured trace 454 (thin grey line) in Fig. 11(c), and an enlarged part of the measured and synthetic traces around the BSR reflection is shown in Fig. 12(a). The overall agreement in amplitude and phase is very good. Discrepancies arise close to the seafloor reflection and are due to the impact of the noise in the data on the sparse spike-train deconvolution. The impedance drop at the BSR seems to be slightly overestimated, again an uncertainty

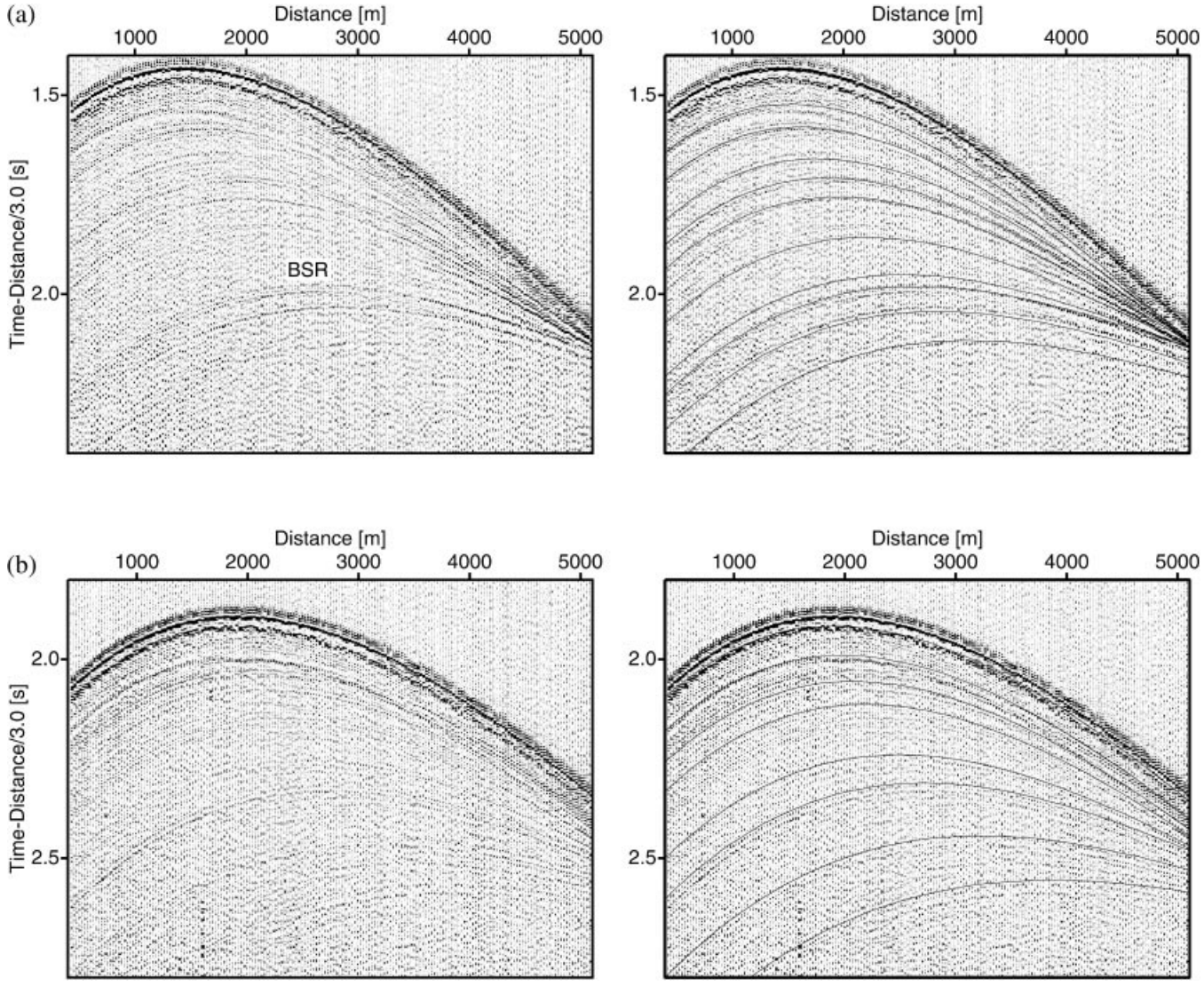

Figure 6. (a) Wide-angle reflections recorded on OBH6, located in the first slope basin. Several wide-angle arrivals can be identified over epicentral distances of up to 5000 m. (b) Wide-angle reflections detected on OBH4 in the abyssal plain. Arrivals can be followed to offsets of up to 6000 m. On the right-hand side, calculated traveltimes are superimposed on the field data.

due to noise in the data. An enlarged segment of the band-limited impedance log is shown in Fig. 12(b): the impedance drop at the BHSZ shows at 4.08 s TWT or 0.75 s TWT below the seafloor. The water depth is 2490 m, and the estimated depth of the BSR below seafloor is, according to Fig. 11(c), about 670 m. The density at that depth according to Minshull & White (1989) is about 2050 kg m^{-3} and is assumed to be approximately constant across the BHSZ. With respect to the sediment properties introduced by Minshull & White, the resulting velocity drop will then have a magnitude of $\sim$200 m s^{-1}. This is a small value compared with the findings of Minshull & White (1989).

Minshull & White (1989) analysed interval velocities from CDP4400 of a multichannel profile located about 40 km northeast of our survey in a water depth of about 1730 m. Interval velocities derived by Minshull & White (1989) from stacking velocities of CDP4400 indicate a velocity drop of magnitude 820 m s^{-1}, from about 2050 m s^{-1} to 1230 m s^{-1}, and a low-velocity zone of about 100 ms TWT.

We computed a band-limited impedance log from their data. Results are given in Fig. 13. Fig. 13(a) shows part of the profile around CDP4400. In a water depth of 1730 m, the BSR appears at 2.82 s TWT (0.54 s TWT below seafloor). The resulting impedance log is shown in Fig. 13(b), and an enlarged part of it in Fig. 14(b). Synthetic and measured data are superimposed in Figs 13(c) and 14(a). Owing to the the very good signal-to-noise ratio in the stacked data, the impedance log can be computed with a resolution of 20 ms, and the agreement of synthetic and measured data is excellent over the whole trace. The BSR impedance drop maps to a depth of about 460 mbsf, where the density is predicted to be 1950 kg m^{-3}. Accordingly, the magnitude of the velocity drop is 470 m s^{-1}, from 2240 m s^{-1} to 1770 m s^{-1}.

The obvious discrepancy between our estimates and those from Minshull & White (1989) can be explained when the absolute minimum of the band-limited impedance below the BSR at 2.94 ms (Fig. 14b) is taken into account, which will influence stacking velocities. With a density of 2050 kg m^{-3},

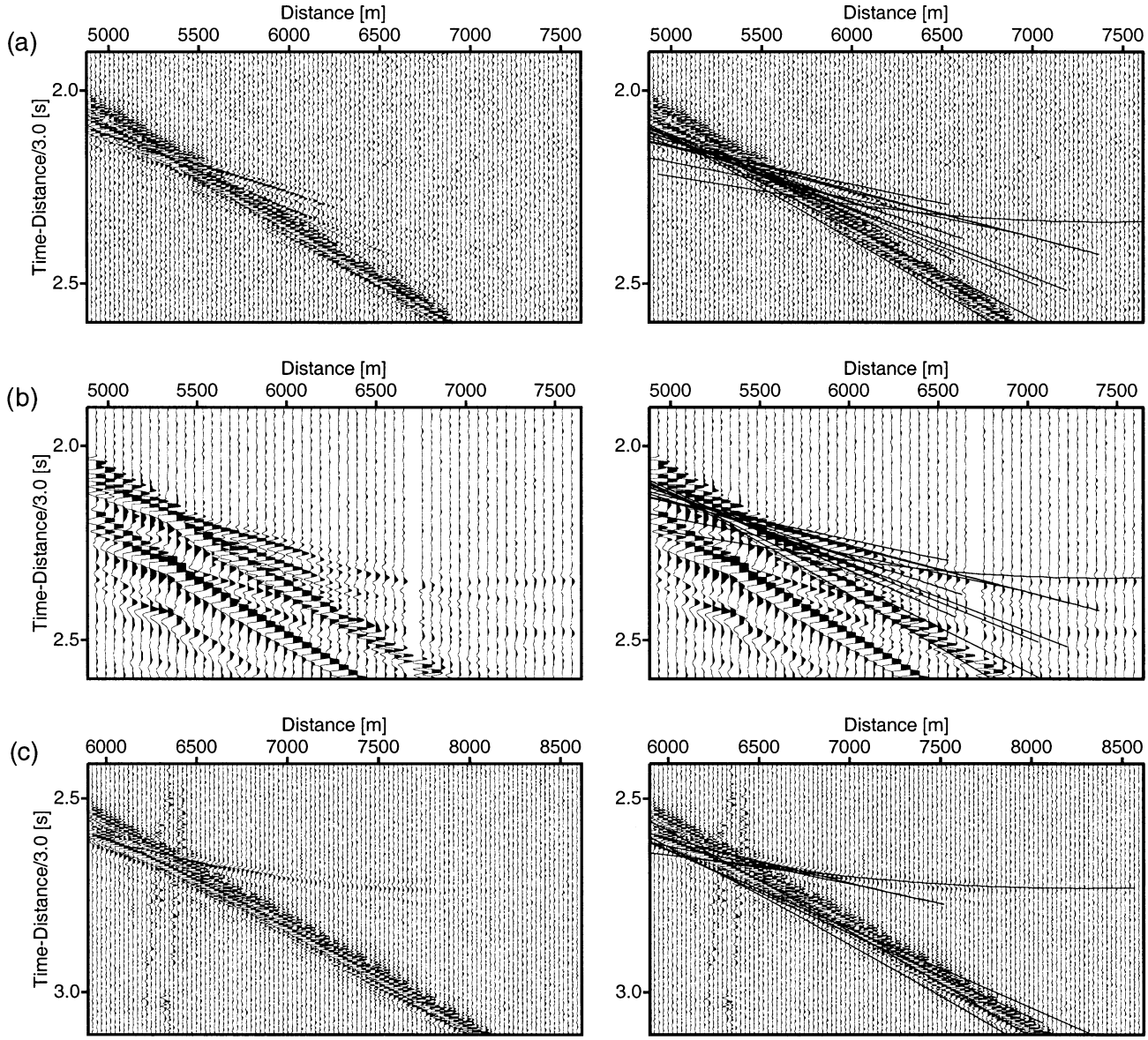

Figure 7. (a) and (b): refracted arrivals recorded on OBH6 on the accretionary wedge. The airgun source was (a) a 2.5-litre GI gun and (b) an 8-litre Prakla gun. The GI gun did not transmit energy to offsets larger than ~6500 m. (c) Refracted arrivals recorded in the abyssal plain on OBH4. On the right-hand side calculated traveltimes are superimposed on the field data.

the velocity drops to 1580 m s^{-1}, yielding a total velocity difference of 660 m s^{-1} which is in better agreement with Minshull & White (1989). The band-limited impedance model from data of Minshull & White (1989) and the derived absolute values of velocities above and immediately below the BSR are consistent with the model of Hyndman & Davis (1992), who estimate an impedance of 4.3×10^6 kg s^{-1} m^{-2} in the HSZ and a velocity of 1900 m s^{-1} (impedance of 3.6×10^6 kg s^{-1} m^{-2}) for the sediments immediately below the BSR in the absence of free gas.

The two data sets are from different water depths, which is reflected in the different depth at which the BSR occurs in our data and in the data of Minshull & White (1989). The substantially lower magnitudes in the drop of impedance at the BHSZ in our data has no unambiguous explanation, although it may indicate hydrate recycling (see discussion below). BSR reflections are relatively small in all our data despite the fact that we used two different sources, a modern 2.5-litre GI airgun as well as an older single-chamber 8-litre airgun that produced higher signal levels in the low-frequency band. Therefore, frequency-dependent attenuation is a very unlikely cause for the observed lower reflection strength in our data. However, a strong amplitude versus offset (AVO) anomaly of the BSR may boost amplitudes in the stacked multichannel data.

DISCUSSION AND CONCLUSIONS

We have presented results from vertical-incidence profiles across the Makran accretionary wedge and from a combined seismic refraction and wide-angle study of sediments within the HSZ off Pakistan. The most prominent feature across the entire continental margin into the Gulf of Oman is a bottom simulating reflector. The OBH data from the accretionary

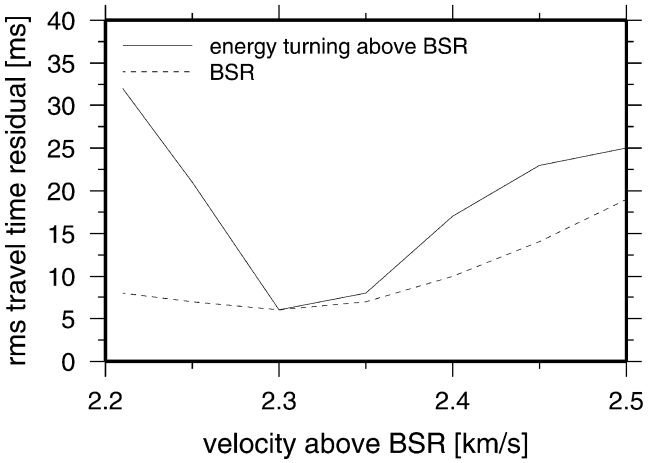

Figure 8. Rms traveltime residuals versus velocity for the hydrate layer above the BSR.

wedge show strong evidence for a low-velocity zone located beneath the BSR. The resultant velocity–depth solution obtained from joint traveltime inversion of wide-angle and refraction data (Fig. 9) indicates a low-velocity zone approximately 200 m thick beneath the BSR. This zone roughly corresponds to the two-way traveltime of the zone of enhanced reflectivity beneath the BHSZ (Fig. 5). This agrees well with observations from the Blake Ridge (Holbrook *et al.* 1996), where vertical seismic profiling (VSP) results indicate an unexpectedly thick (at least 200–250 m) zone of free gas. Based on results from ODP leg 164, Holbrook *et al.* (1996) were able to show that the reflectivity seen at and beneath the BSR indicates layers containing trapped gas in pore fluids. Gas is expected to concentrate along stratigraphic layers because of slight changes in permeability across layer boundaries. Even at low concentrations, slight variations of gas content lead to strong fluctuations of *P* velocities and therefore to enhanced reflectivity. This observation contradicts earlier ideas which suggested that there is amplitude blanking above the BSR, a phenomenon interpreted in terms of the presence of gas hydrate (Dillon *et al.* 1993). However, Holbrook *et al.* (1996) demonstrated that the low reflectivity in the HSZ on the Blake Ridge is caused by very uniform sediments. Therefore, the reflectivity pattern in the Blake Ridge is normal above the BSR but shows enhanced reflectivity beneath it. Thus, gas hydrates apparently do not cause a reduction of reflectivity.

Nevertheless, with respect to a single gradient background model, the joint traveltime inversion yielded higher velocities immediately above the BSR. The increase in seismic velocity may represent the replacement of pore fluid with solid gas hydrate (e.g. Hyndman & Spence 1992; Yuan *et al.* 1996). However, even a change in lithology may support higher velocities. Therefore it is difficult to assess the amount of gas hydrate stored within the sediments. The difference between the reference and observed velocities (of about 100 m s^{-1}) suggests that only a few percent of pore space is occupied by solid gas hydrate. The low-velocity zone and the increase in reflectivity beneath the HSZ, however, seem to correspond to free gas trapped beneath the BSR (e.g. Minshull & White 1989; Miller *et al.* 1991; Yuan *et al.* 1996).

Simple traveltime analysis is generally not appropriate to constrain the velocity structure of an inversion zone. We

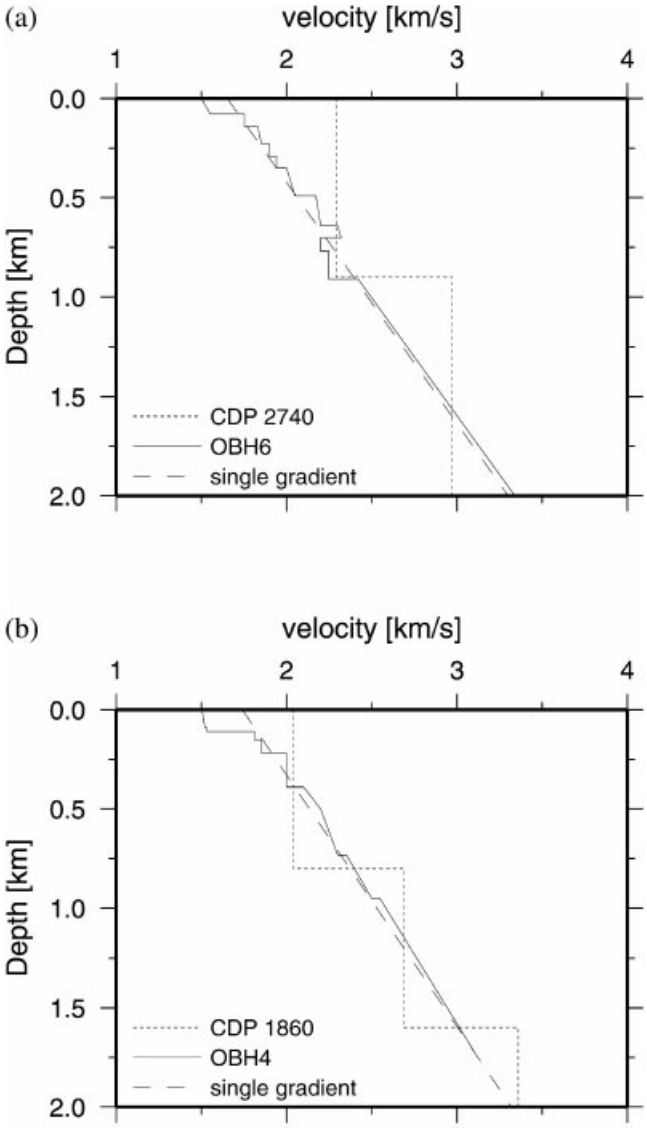

Figure 9. Velocity–depth solutions from traveltime inversion of wide-angle reflections and refraction data. CDP2740 and 1860 are the velocities derived from reflection data by Frühn *et al.* (1997). (a) Solution for line 9707 on the accretionary complex. (b) Solution from the Gulf of Oman.

therefore computed band-limited impedance logs from deconvolved and scaled reflection data, yielding a velocity drop of $\sim$200 m s^{-1} at BSR depth. The same technique applied to the reflection data collected by Minshull & White (1989) provided a drop in velocity of about 600 m s^{-1}. The two study areas are only some 40 km apart, suggesting that BSR characteristics vary significantly over the Makran margin. While the Minshull & White (1989) data may suggest the presence of widespread free gas, only small quantities of free gas can exist below the BSR sampled during our survey. This idea is supported by the wide-angle data. The presence of free gas would produce a strong AVO anomaly. The OBH data (Fig. 6), however, do not display AVO characteristics associated with the presence of large quantities of free gas below the HSZ, as for example detected by Katzman *et al.* (1994). In addition, Minshull & White (1989) obsevered reflection amplitudes of almost 60 per cent for the BSR with respect to the seafloor reflection, while

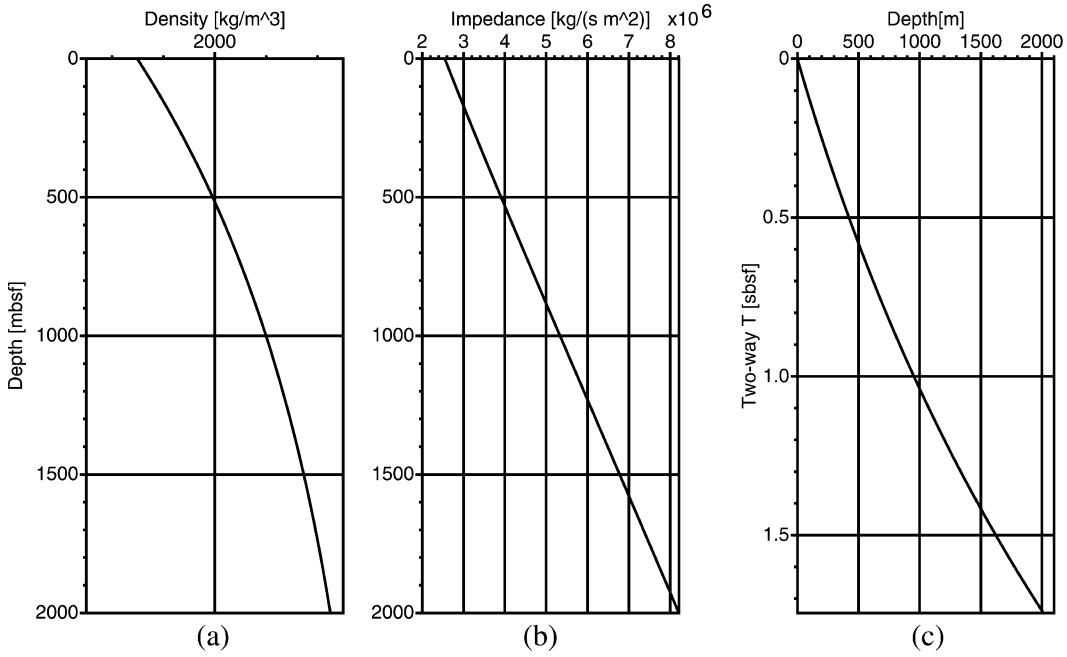

Figure 10. (a) Density versus depth derived from a porosity/depth relationship for the Makran accretionary wedge given by Minshul & White (1989). (b) Background impedance computed from data in (a) and background velocities from OBH data (see Fig. 9a). (c) Two-way traveltime versus depth according to the background velocity model in Fig. 9(a).

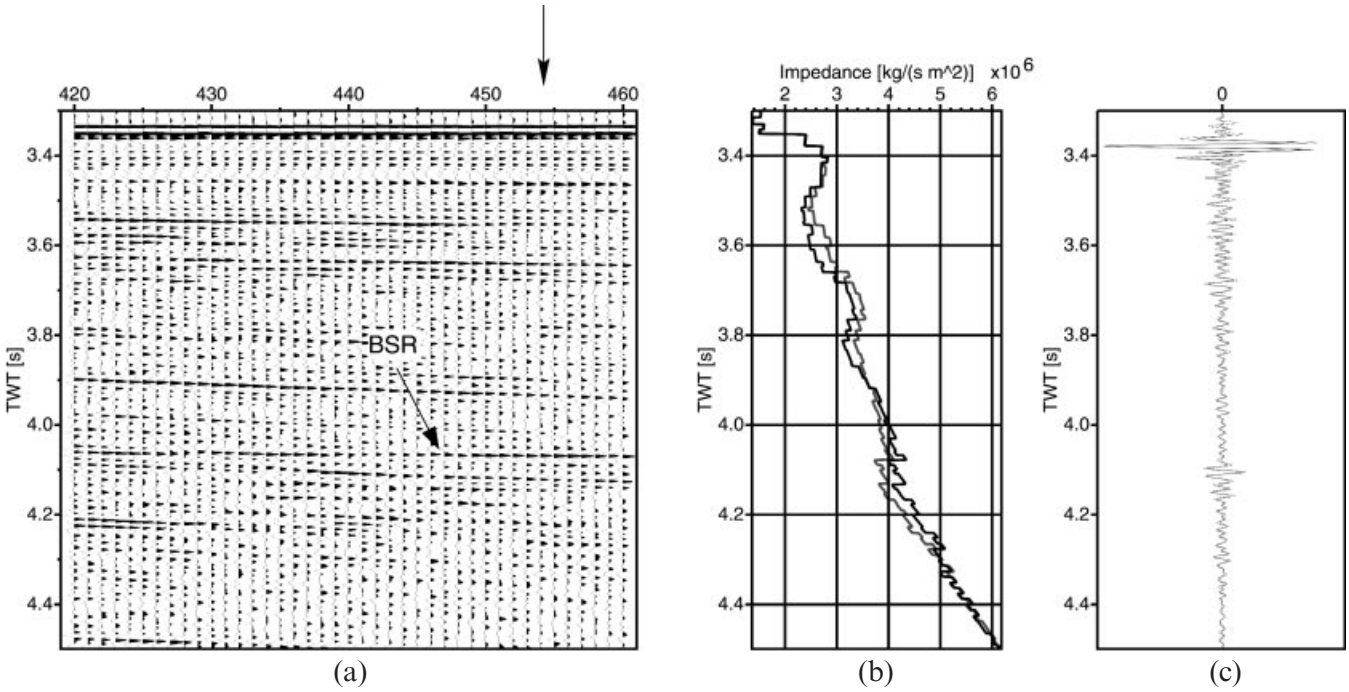

Figure 11. (a) Subset of our vertical incidence data in the vicinity of the OBH positions. The arrow marks the traces selected for the computation of the band-limited impedance logs in (b). (b) Band-limited impedance logs of traces 454 and 455. Small trace-to-trace discrepancies are mostly due to noise in the data. (c) Real trace (solid line) with synthetic trace computed from the band-limited impedance log of trace 454 (dotted line) superimposed. Minor discrepancies arise close to the sea-bottom reflection.

amplitudes of the BSR in our reflection data do not exceed 25 per cent of the amplitude from the seafloor reflection. Although Fink & Spence (1999) found that BSR reflection coefficients are slightly larger for 30-Hz data (10–60 Hz for the Minshull & White 1989 data) than for 75-Hz data (30–85 Hz for our data), the striking differences in reflection amplitudes indicate that BSR properties are profoundly different. However, we note that Holbrook *et al.* (1996) have pointed out that the amplitude of the BSR is controlled by local concentrations of methane gas in thin (< 20 m) layers and is not directly related to the total amount of free gas present beneath the HSZ, nor is it related to the amount of hydrate present above the BSR.

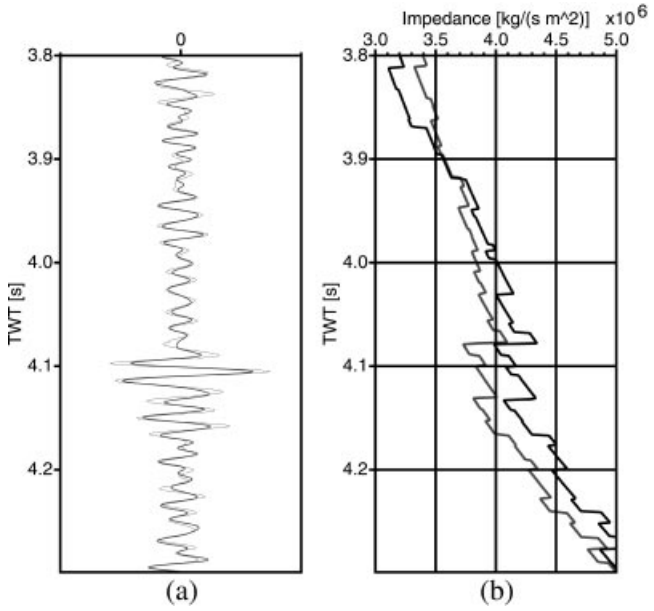

Figure 12. (a) Close up of real (solid line) and synthetic trace (dotted line) around the BSR reflection at 4.1 s TWT. (b) Close up of the band-limited impedance logs of traces 454 and 455 around the BSR impedance drop.

In the abyssal plain, the OBH data did not display evidence for a low-velocity layer at BSR depth, although in the vertical-incidence measurements a reflector with reverse polarity is present (Fig. 4f). The event occurs at a similar depth to where White (1977) and Minshull & White (1989) sampled seismic 'bright spots'. Furthermore, it cuts across the seismic strata and is therefore interpreted as the BSR. Compared with the seismic stratigraphy above and below, its reflection amplitude is 'normal'. Thus the reflector is not associated with a strong decrease in acoustic impedance. In addition, sediments below the BSR are not characterized by enhanced reflectivities and thus do not indicate the presence of large quantities of free gas. Consistently, wide-angle data did not show a prominent reflection, and seismic refraction data could be easily approximated by a single vertical velocity gradient. We therefore conclude that the amount of methane stored in sediments of the Gulf of Oman is much less than within sediments from the accretionary wedge.

The occurrence of gas hydrates in nature is controlled by a function of the temperature, pressure and composition of the gas (Kvenvolden 1993), although another feature of gas hydrate occurrence is the amount of gas (methane) that is necessary for gas hydrate formation. Because the solubility of methane in sea water is very low, the amount of methane required for gas hydrates greatly exceeds the solubility of methane in water (Kvenvolden 1993), suggesting that gas hydrate formation is confined to regions where a significant amount of methane is supplied from elsewhere. The sites studied are only 20–40 km apart; thus, profound differences in sediment composition are unlikely. We therefore conclude that hydrate recycling (Kvenvolden 1993; Paull *et al.* 1994; Pecher *et al.* 1996, 1998; von Huene & Pecher 1999) must be a key factor controlling the appearance of the BSRs across the Makran active continental margin.

To facilitate the discussion, we briefly introduce the idea of hydrate recycling. A continuation of sedimentation and subsequent subsidence of the underlying sediment and/or tectonic uplift cause new temperature and pressure conditions, which will shift the isotherms and hence the BHSZ upwards. If gas hydrates are already present, they will dissociate into free gas. The buoyancy of the free gas causes an upward migration and hydrates will appear again when the rising gas re-enters the

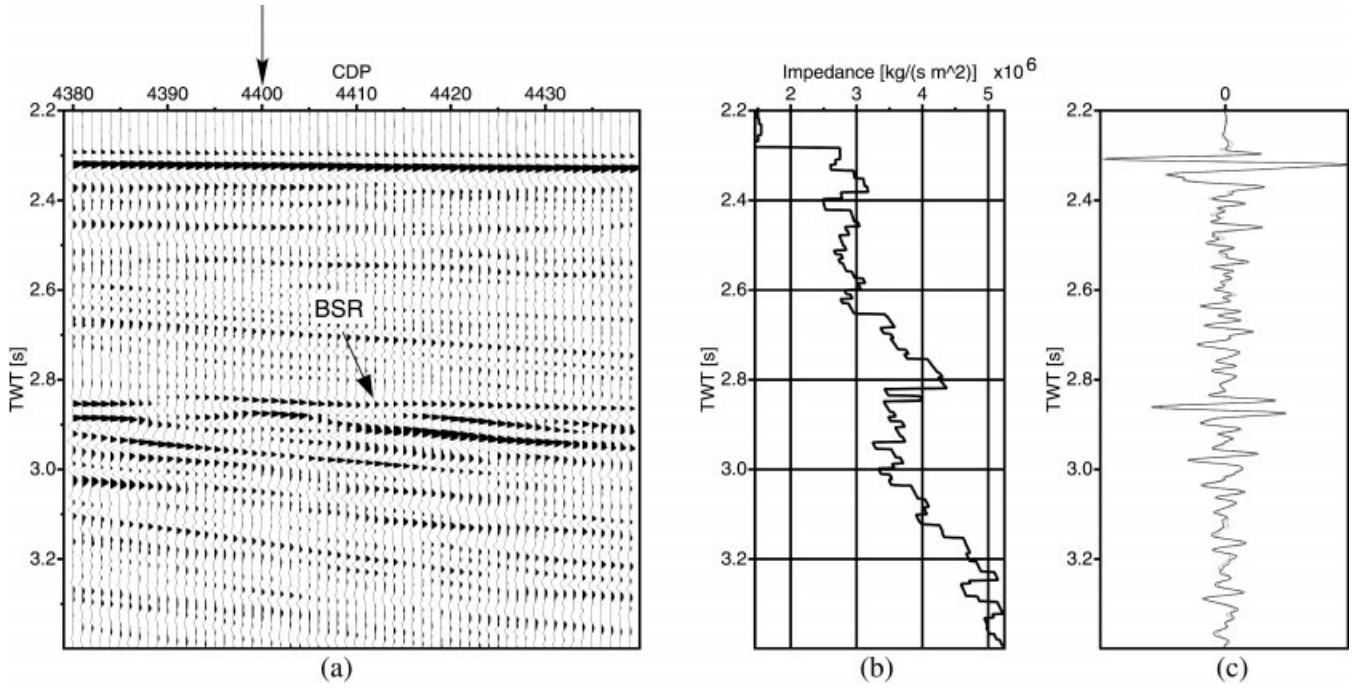

Figure 13. (a) Subset of the stacked multichannel line CAM30 of Minshul & White (1989). CDP4400 selected for the computation of the band-limited impedance log in (b) is marked with an arrow. (b) Band-limited impedance log of CDP4400. (c) Real trace (solid line) with synthetic trace (dotted line) superimposed. Owing to an excellent signal-to-noise ratio, agreement in phase and amplitude is excellent.

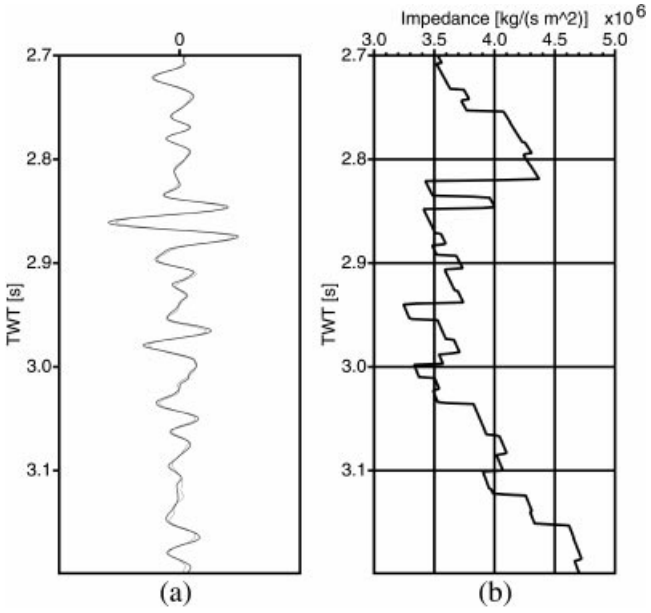

Figure 14. (a) Close up of real (solid line) and synthetic trace (dotted line) around the BSR reflection at 2.85 s TWT. (b) Close up of the band-limited impedance logs of CDP4400 from the CAM30 line around the BSR impedance drop.

new HSZ or it will accumulate as free gas beneath. On the other hand, subsidence and erosion suppress BSRs, because a downward movement of the HSZ traps gas hydrates (Pecher *et al.* 1998; von Huene & Pecher 1999). Across the Makran accretionary prism, however, BSRs are prominent within slope basins, and tectonic uplift dominates the morphotectonics of the accretionary complex (White & Louden 1982; Minshull & White 1989). Therefore, subsidence and erosion may be insignificant, although the accumulation of sediments on accretionary ridges and their potential for slumping and resedimentation may generate debris flows from ridges into adjacent slope basins. This process, however, would also cause hydrate recycling.

We think that the variations in BSR appearance are related to an evolutionary process. Within the abyssal plain the BSR amplitude is weak, indicating that only very small quantities of free gas are present beneath, although locally free gas may accumulate and form bright spots (White 1977; Minshull & White 1989). Approaching the accretionary complex, sediments become folded at the deformation front and subsequently uplifted as they are incorporated into the accretionary prism. Uplift and ongoing sedimentation will produce gas hydrate recycling. Thus, at least small quantities of free gas have accumulated beneath the BSR imaged within the first slope basin, as indicated along line 9707 by the low-velocity zone at BSR depth and an increase in reflectivity beneath. Farther landwards, tectonic forces and ongoing sedimentation have again uplifted and buried the slope basins. In turn, the BHSZ has been shifted upwards and hydrate recycling has caused an enhancement of the BSR. This fact is clearly indicated by the properties found at CDP4400 of Minshull & White (1989), where free gas may be widespread beneath the BSR. To summarize, with time (i.e. going from the abyssal plain landwards) ongoing sedimentation and uplift produce an enhancement of the BSR by the accumulation of hydrate and/or free gas at the BHSZ by hydrate recycling. Consequently, sedimentation and tectonic uplift are key factors which control BSR characteristics off Pakistan.

In addition, hydrate may accumulate at the BHSZ due to the advection of methane from depth. Fluid migration is a common feature of active continental margins (e.g. Suess *et al.* 1998). Approaching the continental margin off Pakistan, seismic studies show a marked change in velocity structure (Minshull & White 1989; Frühn *et al.* 1997). Minshull & White (1989) interpreted this phenomenon in terms of porosity reduction as pore fluids are squeezed out of compacting sediments. Even the reflection seismic images presented in this paper may indicate fluid circulation. At locations where the BSR reflector cuts across the strata, depth variations of the BSR are common. Because the BSR depth depends on pressure and temperature conditions, we suggest that pore water migration along lithological boundaries or fault zones may disturb the temperature field where fluids approach the BHSZ. Most profoundly, and already mentioned by Minshull *et al.* (1992), is this phenomenon on the landward side of slope basins, where the BSR curves upwards (Figs 2 and 4b). However, it also occurs elsewhere (compare Figs 4a and d with e). To calculate the advective accumulation of methane, Rempel & Buffett (1997) derived a theoretical expression. Using typical estimates of fluid velocities in accretionary environments, they obtain an accumulation rate of 1 per cent of the pore volume in 10^5 years.

ACKNOWLEDGMENTS

Thorough reviews by Anne Tréhu and Ingo Pecher are greatly appreciated and substantially improved an earlier version of this manuscript. We thank Wilfried Weigel for his generous support and his substantial role in planning the cruise, Oliver Dahlmann, Olaf Exner, Bernd Heesemann, Björn Herber, Rolf Herber and Hermann Richter for assistance at sea, and master Andresen and his crew of RV *Sonne* for their assistance and cooperation. Ernst Flüh provided housings for the ocean bottom hydrophones, Bob White and Jürgen Frühn kindly provided CDP4400 of the CAM30 line, and Nina Kukowski compiled the swathmapping bathymetry shown in Fig. 1. We are grateful to the Government of Pakistan for opening territorial waters. This work was supported by the Bundesminister für Bildung, Wissenschaft, Forschung und Technologie (grant 03G0124A) and IG by the Deutsche Forschungsgemeinschaft (grant Vi 133/3).

REFERENCES

Clayton, R.W. & Stolt, R.H., 1981. A Born-WKBJ inversion method for acoustic reflection data, *Geophysics,* **46,** 1559–1567.

Dietrich, M. & Kormendi, F., 1990. Pertubation of the plane wave reflectivity of a depth dependent elastic medium by weak inhomogeneities, *Geophys. J. Int.,* **100,** 203–214.

Dillon, W.P., Lee, M.W., Fehlhaber, K. & Coleman, D.F., 1993. Gas hydrates on the Atlantic continental margin of the United States—Controls on concentration, in *The Future of Energy Gases,* pp. 313–330, ed. Howell, D.G., US Geol. Surv., Reston, VA.

Dorau, F., 1991. Eindimensionale Inversion bandbegrenzter Seismogramme, *Berichte aus dem Zentrum für Meeres- und Klimaforschung,* **16,** University of Hamburg.

Fink, C.R. & Spence, G.D., 1999. Hydrate distribution off Vancouver Island from multifrequency single-channel seismic reflection data, *J. geophys. Res.,* **104,** 2909–2922.

Frühn, J., White, R.S. & Minshull, T.A., 1997. Internal deformation and compaction of the Makran accetionary wedge, *Terra Nova,* **9,** 101–104.

Holbrook, W.S., Hoskins, H., Wood, W.T., Stephen, R.A., Lizarralde, D. & Leg 164 Science Party, 1996. Methane hydrate and free gas on the Blake Ridge from vertical seismic profiling, *Science,* **273,** 1840–1843.

Hutchison, I., Louden, K.E., White, R.S. & von Herzen, R.P., 1981. Heat flow and age in the Gulf of Oman, *Earth planet. Sci. Lett.,* **56,** 252–262.

Hyndman, R.D. & Davis, E.E., 1992. A mechanism for the formation of methane hydrate and seafloor bottom simulating reflectors by vertical fluid expulsion, *J. geophys. Res.,* **97,** 7025–7041.

Hyndman, R.D. & Spence, G.D., 1992. A seismic study of methane hydrate marine bottom simulating reflectors, *J. geophys. Res.,* **97,** 6683–6698.

Katzman, R., Holbrook, W.S. & Paull, C.K., 1994. Combined vertical-incidence and wide-angle seismic study of a gas hydrate zone, Blake Ridge, *J. geophys. Res.,* **99,** 17 975–17 995.

Kaul, N., Rosenberger, A. & Villinger, H., 2000. Comparsion of measured and BSR-derived heat flow values, Makran accretionary prism, Pakistan, *Mar. Geol.,* in press.

Korenga, J., Holbrook, W.S., Singh, S.C. & Minshull, T.A., 1997. Natural gas hydrates on the southeast U.S. margin: Constraints from full waveform and travel time inversions of wide-angle seismic data, *J. geophys. Res.,* **102,** 15 345–15 365.

Kukowski, N., Schillhorn, T., Flueh, E.R., Huhn, K. & MAMUT working group, 2000. A newly identified transform plate boundary through the Makran accretionary wedge, *Geology,* submitted.

Kvenvolden, K.A., 1993. Gas hydrates—Geological perspective and global change, *Rev. Geophys.,* **31,** 173–187.

Lavergne, M. & Willm, C., 1977. Inversion of seismograms and pseudo velocity logs, *Geophys. Prospect.,* **25,** 231–250.

Lee, W.M., Hutchison, D.R., Agena, W.F., Dillon, W.P., Miller, J.J. & Swift, B.A., 1994. Seismic character of gas hydrates on the southeast U.S. continental margin, *Mar. geophys. Res.,* **16,** 163–184.

Levy, S. & Fullagar, P.K., 1981. Reconstruction of a sparse spike train from a portion of its spectrum and application to high-resolution deconvolution, *Geophysics,* **9,** 1235–1243.

Miller, J.J., Lee, M.W. & von Huene, R., 1991. An analysis of a seismic reflection from the base of a gas hydrate zone, offshore Peru, *AAPG Bull.,* **75,** 910–924.

Minshull, T.A. & White, R.S., 1989. Sediment compaction and fluid migration in the Makran accretionary prism, *J. geophys. Res.,* **94,** 7387–7402.

Minshull, T.A., White, R.S., Barton, P.J. & Collier, J.S., 1992. Deformation at plate boundaries around the Gulf of Oman, *Mar. Geol.,* **104,** 265–277.

Minshull, T.A., Singh, S.C. & Westbrook, G.K., 1994. Seismic velocity structure at a gas hydrate reflector, offshore Columbia, from full waveform inversion, *J. geophys. Res.,* **99,** 4715–4734.

Paull, C.K. & Dillon, W.P., 1981. Appearance and distribution of the gas hydrate reflection in the Blake Ridge region, offshore southeastern United States, *US Geol. Surv. Misc. Field Stud. Map,* MF-1252.

Paull, C.K., Ussler, W. III & Borowski, W.S., 1994. Sources of biogenic methane to form marine gas hydrates, *Ann. NY Acad. Sci.,* **15,** 392–411.

Pecher, I.A., Minshull, T.A., Singh, S.C. & von Huene, R., 1996. Velocity structure of a bottom simulating reflector offshore Peru: results from full waveform inversion, *Earth planet. Sci. Lett.,* **139,** 459–469.

Pecher, I.A., Ranero, C.R., von Huene, R., Minshull, T.A. & Singh, S.C., 1998. The nature and distribution of bottom simulating reflectors at the Costa Rician continental margin, *Geophys. J. Int.,* **133,** 219–229.

Rempel, A.W. & Buffett, B.A., 1997. Formation and accumulation of gas hydrate in porous media, *J. geophys. Res.,* **102,** 10 151–10 264.

Singh, S.C., Minshull, T.A. & Spence, G.D., 1993. Velocity structure of a gas hydrate reflector, *Science,* **260,** 204–207.

Sloan, E.D., 1990. *Clathrate Hydrates of Natural Gas,* Marcel Dekker, New York.

Suess, E., Bohrmann, G., von Huene, R., Linke, P., Wallmann, K., Lammers, S., Sahling, H., Winckler, G., Lutz, R.A. & Orange, D., 1998. Fluid venting in the eastern Aleutian subduction zone, *J. geophys. Res.,* **103,** 2597–2614.

von Huene, R. & Pecher, I.A., 1999. Vertical tectonics and orgins of BSRs along the Peru margin, *Earth planet. Sci. Lett.,* **166,** 47–55.

Whalley, E., 1980. Speed of longitudinal sound in clathrate hydrates, *J. geophys. Res.,* **85,** 2539–2542.

White, R.S., 1977. Seismic bright spots in the Gulf of Oman, *Earth planet. Sci. Lett.,* **73,** 29–37.

White, R.S. & Klitgord, K., 1976. Sediment deformation and plate tectonics in the Gulf of Oman, *Earth planet. Sci. Lett.,* **32,** 199–209.

White, R.S. & Louden, K.E., 1982. The Makran continental margin: Structure of a thickly sedimented convergent plate boundary, in *Studies in Continental Margin Geology,* eds Watkins, J.S. & Drake, C.L., *Mem. Am. Assoc. Pet. Geol.,* **34,** 499–518.

Yuan, T., Hyndman, R.D., Spence, G.D. & Desmons, B., 1996. Seismic velocity increase and deep sea gas hydrate concentration above a bottom simulating reflector on the northern Cascadia continental slope, *J. geophys. Res.,* **101,** 13 655–13 671.

Zelt, C.A. & Smith, R.B., 1992. Seismic travel time inversion for 2-D crustal velocity structure, *Geophys. J. Int.,* **108,** 16–34.

APPENDIX A: BAND-LIMITED IMPEDANCE LOGS FROM SINGLE-CHANNEL DATA

The number of constraints available from single-channel vertical-incidence seismic data is in general too limited for any inversion scheme. By our definition, seismic inversion attempts to find a global optimum of a misfit function between measured data and data from a forward model calculated from all relevant physical parameters of the inversion result, with depth as the independent variable. Obviously the only physical parameter that single-channel vertical-incidence seismograms can be inverted for is an impedance versus traveltime function.

For the analysis of single-channel near-vertical-incidence data we therefore propose a signal processing scheme described in Dorau (1991). The final result of this algorithm is band-limited impedance logs, which removes much of the burden of dealing with waveforms, resolution and interference artefacts in the analysis of BSR reflection strength. The advantage of band-limited impedance logs is in fact that their limitations are concise and unambiguous. Any conclusions drawn from band-limited impedance logs can be referenced to that framework of quantifiable limitations.

Rather than giving a review of Dorau (1991) we will demonstrate the processing sequence along with its limitations on a synthetic example.

In Fig. A1(a) an impedance versus depth function is shown that exhibits the characteristics of a simple BSR model (e.g. Hyndman & Davis 1992). For the sake of clarity, this model has only two discontinuities, one at the ocean bottom and the other one at the base of the hydrate layer. We use a plane wave, normal-incidence algorithm to calculate a synthetic seismogram to which noise is added yielding a signal-to-noise ratio of 20 (with respect to power spectral density). The wavelet used is a four-peak damped sinusoid (Fig. A1b). As in a normal

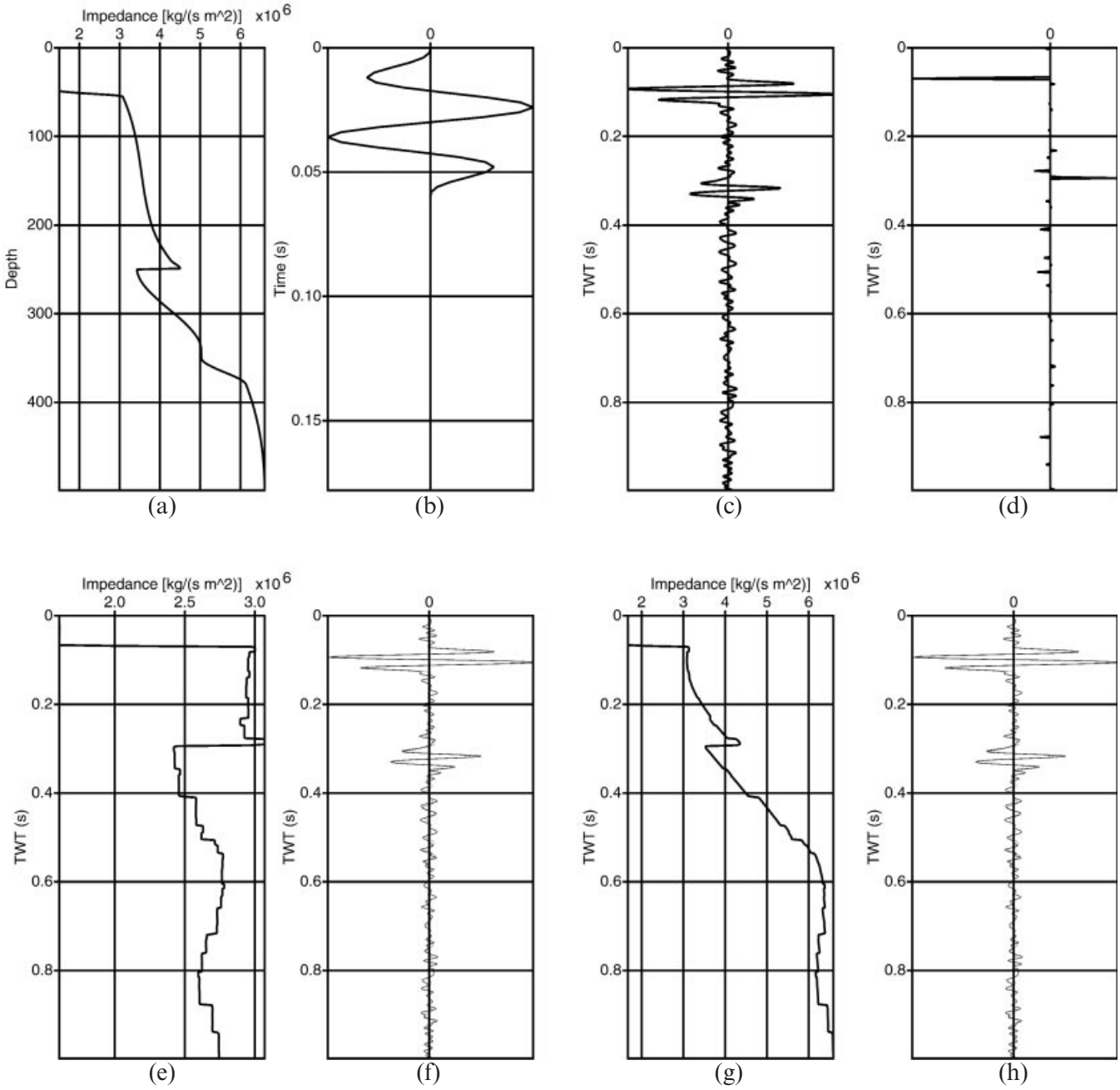

Figure A1. (a) Model of impedance versus depth for a generalized BSR. (b) The wavelet used for the computation of the sythetic seismogram in (c) is a damped sinusoid. (c) Synthetic seismogram contaminated with noise, signal-to-noise ratio = 20. (d) Reflectivity function recovered by sparse spike-train deconvolution. (e) Band-limited impedance log without background impedance model. (f) Synthetic seismogram (continuous line) computed from band-limited impedance in (e) superimposed on original data (dotted line) as shown in (c). (g) Band-limited impedance log combined with background impedance. Note, that by comparison with (a), data here are on a time scale. (h) Synthetic seismogram (continuous line) computed from band-limited impedance as shown in (g) superimposed on original data (dotted line) as shown in (c). Both impedance logs in (e) and in (g) correspond to almost identical synthetic traces in (g) and (h), respectively.

processing sequence, the resultant seismogram is low-pass filtered. The result is shown in Fig. A1(c).

This seismogram is now subjected to the deconvolution algorithm of Levy & Fullagar (1981). This is an L1-norm algorithm where the number of spikes in the deconvolved trace is minimized subject to the constraint that the deconvolved trace matches a band $f_1 < f < f_2$ of the complex spectrum of the original data weighted by the inverse complex wavelet spectrum.

With noisy data the usable bandwidth will always be smaller than that of the original data, and thus the resolution of the deconvolved trace which may be quantified in the time domain as $1/(f_2 - f_1)$ s cannot be better than the original data. A source wavelet must be known within those spectral limits or has to be estimated from the data. It is obvious that the sparse spike-train deconvolved trace will only contain contributions from impedance discontinuities. All information from higher-order impedance changes is lost. Actually, this information is

constrained to the low-frequency part of the reflectivity function and is lost already due to the bandpass-filter properties of the wavelet. Whatever may be left is small in amplitude and unretrievably buried in the noise. The algorithm of Levy and Fullagar is generally robust in the presence of noise. In our example, however, a signal-to-noise ratio of 20 was about the limit for which a proper result could be obtained. Tolerance towards higher noise levels is traded against resolution. In the limit, a single spike will split into one or more spikes of similar or opposite polarity.

The wavelet used for the synthetic trace in Fig. A1(c) is originally band-limited from 20 to 60 Hz. For the sparse spike-train deconvolution, we used the spectrum of the seismogram from 30 to 50 Hz for the constraints. The upper bound on time resolution in the deconvolved trace is thus 50 ms, and the result is shown in Fig. A1(d).

If an arbitrary impedance function is modelled as a constant (background) impedance function plus some disturbance, a simple integral (Dorau 1991) can be derived from the Born expansion (Lavergne & Willm 1977; Clayton & Stolt 1981; Dietrich & Kormendi 1990) which will recover an impedance function from a reflectivity series

$$\Gamma(t) = \Gamma_0 \exp\left[2 \int_0^t R(\tau)\, d\tau \right], \tag{A1}$$

where Γ_0 is the constant background impedance, $R(t)$ the reflectivity, $\Gamma(t)$ the impedance function and t the two-way traveltime. Given a clean, zero-noise reflectivity function, an iterative scheme can in fact retrieve the impedance function with arbitrary precision.

In our case the reflectivity series is the result of band-limited deconvolution and contamination with noise. Thus the result of the evaluation of eq. (A1) will suffer the limitations inherited from the deconvolution: low-frequency trends are lost and resolution is limited to 50 ms. In fact, the result in Fig. A1(e) bears little resemblance to the true impedance function in Fig. A1(a). The relative sizes of the first-order impedance contrasts, however, are well recovered, and provided that the ocean bottom impedance contrast was estimated correctly, the size of the impedance drop at the base of the hydrated zone relative to the ocean bottom impedance contrast can be quantified.

This is demonstrated in Fig. A1(f), where we used the band-limited impedance log from Fig. A1(e) to compute a synthetic seismogram (black line) and compare that with the initial data (dotted line). The band-limited impedance log is in fact a valid model since the synthetic seismogram associated with it matches the initial data very well. Any continuous (smooth) background impedance model can now be combined with the pseudo impedance from Fig. A1(e) and still produce the same forward seismogram. This addresses the core problem of seismic inversion and is illustrated in Fig. A1(g), where we combined the band-limited impedance log with a smooth sigmoid-type impedance function. The resulting function resembles that of Fig. A1(a) much more closely, while the forward seismogram in Fig. A1(h) is indistinguishable from that in Fig. A1(f).

While we could have attempted to estimate reflection coefficients directly from signal amplitudes in the data and use the Born approximation implicitly in our method to estimate impedance (e.g. Lee *et al.* 1994), we think that the advantage of a processing sequence with clearly stated assumptions with respect to the source wavelet, a quantifiable resolution and comprehensive limitations of the result is obvious.